Computers & Geosciences 56 (2013) 151–160

Contents lists available at SciVerse ScienceDirect

Computers & Geosciences

journal homepage: www.elsevier.com/locate/cageo

NETVOLC: An algorithm for automatic delimitation of volcano edifice boundaries using DEMs

Leonardo D. Euillades [a,*], Pablo Grosse [b], Pablo A. Euillades [a]

[a] CONICET and Instituto CEDIAC, Facultad de Ingeniería, Universidad Nacional de Cuyo, cc 405, Centro Universitario, (M5502JMA) Ciudad de Mendoza, Mendoza, Argentina

[b] CONICET and Fundación Miguel Lillo, Miguel Lillo 251, (T4000JFE) San Miguel de Tucumán, Tucumán, Argentina

ARTICLE INFO

Article history:
Received 14 December 2012
Received in revised form
11 March 2013
Accepted 12 March 2013
Available online 22 March 2013

Keywords:
Morphometry
Volcano landform
Digital elevation model
Minimum cost flow networks

ABSTRACT

Accurately delimiting boundaries is required for characterizing landforms through measurement of their geomorphometric parameters. Volcanism produces a wide range of landforms, from symmetric cones to very irregular massifs, that can gradually merge with the surroundings and contain other elements, thus complicating landform delimitation. Most morphometric studies of volcanoes delimit landforms manually, with the inconvenience of being time-consuming and subjective. Here we propose an algorithm, NETVOLC, for automatic volcano landform delimitation based on the premise that edifices are bounded by concave breaks in slope. NETVOLC applies minimum cost flow (MCF) networks for computing the best possible edifice outline using a DEM and its first- and second-order derivatives. The main cost function considers only profile convexity and aspect; three alternative functions (useful in complex cases) also consider slope, elevation and/or radial distance. NETVOLC performance is tested by processing the Mauna Kea pyroclastic cone field. Results using the main cost function compare favorably to manually delineated outlines in 2/3rds of cases, whereas for the remaining 1/3rd of cases an alternative cost function is needed, introducing some degree of subjectivity. Our algorithm provides a flexible, objective and time-saving tool for automatically delineating volcanic edifices. Furthermore, it could be used for delineating other landforms with concave breaks in slope boundaries. Finally, straightforward modifications can be implemented to extend the algorithm capabilities for delimiting landforms bounded by convex breaks in slope, such as summit craters and calderas.

1. Introduction

Landforms are discrete features of the continuous land surface having characteristic, recognizable shapes (Evans, 1972; Neuendorf et al., 2005). Quantitative landform mapping and analysis (specific geomorphometry) is an important task of geomorphology. To measure geometric characteristics of individual landforms, complete delimitation by a closed boundary is necessary. Currently, most landform delimitation is performed manually by visual identification and digitization on maps, airphotos, satellite images or digital elevation models (DEMs) (Evans, 2012). Many landforms are bounded by changes in slope gradient (breaks in slope). The general approach for delimitation of these landforms is manual tracing of slope breaks using DEM-based techniques (Smith and Clark, 2005; Evans, 2012). However, manual delimitation is time-consuming and subject to user subjectivity. Algorithms for automatic boundary delimitation of landforms are thus desirable, but remain a research frontier (Evans, 2012). In recent years, several automatic and semi-automatic approaches have been developed for general landform classification (Bue and Stepinski, 2006; Drăguţ and Blaschke, 2006; Iwahashi and Pike, 2007; Schneider and Klein, 2010) and for extraction of specific landforms, such as seamounts (Hillier, 2008) or drumlins (Saha et al., 2011).

Volcanism produces a wide range of landforms. They can be excavational (calderas, maars) or, more commonly, constructional (monogenetic cones and domes; polygenetic or composite volcanoes). The ideal constructional volcano is a cone with radial symmetry and slopes steeper than its surroundings; it is thus bounded by concave breaks in slope at its base. However, volcanoes tend to exhibit various degrees of complexity, up to very irregular volcanic chains or massifs. In addition, volcanoes can contain several landform elements such as summit craters, small parasitic cones, collapse scars, erosional channels or valleys, ridges, etc. A further complication is that volcanoes tend to merge gradually with the surrounding landscape and some products can be deposited at great distances from the central source. All this makes volcanic landform delimitation for geomorphometric analysis a complicated endeavor. Consequently, most volcano morphometric studies have focused on monogenetic scoria cones

* Corresponding author. Tel.: +54 261 4135000x2108; fax: +54 261 4380120.
E-mail address: leuillades@cediac.uncu.edu.ar (L.D. Euillades).

0098-3004/$ - see front matter © 2013 Elsevier Ltd. All rights reserved.
http://dx.doi.org/10.1016/j.cageo.2013.03.011

because of their simpler morphologies with clearer boundaries (Favalli et al., 2009; Kervyn et al., 2012 and references therein). Morphometric studies of composite volcanoes are relatively few and have used different manual delimitation methods based on product extent (geology), elevation contours and/or breaks in slope (Pike, 1978; Plescia, 2004; Grosse et al., 2009; Völker et al., 2011; Karátson et al., 2012). Recently, Grosse et al. (2012) developed a manual delimitation method using DEM-derived curvature and slope data; they emphasized that delimitation by DEMs should be restricted to volcano edifices and not include their aprons which do not have a clear morphometric signature and tend to merge with the surroundings.

Automatic closed-contouring algorithms, based on searching for the lowest elevation contour with a quasi-elliptical shape that completely encloses a topographic high, have been used to detect and delineate seamounts (Behn et al., 2004; Bohnenstiehl et al., 2008). This method has a major limitation in that closed-contours lie at constant topographic elevation, leading to erroneous solutions when the landform lies on a sloping landscape. Bohnenstiehl et al. (2012) overcome this limitation by implementing a modification to the closed-contouring approach (MBOA) that adjusts base elevation by evaluating the area/perimeter ratio along radial profiles. Application of the MBOA algorithm to a cinder cone field shows that it performs much better than the standard closed-contour method (Howell et al., 2012). However, it depends on several user-defined parameters and thresholds, introducing some degree of subjectivity.

Here we present the algorithm NETVOLC for automatic delimitation of volcano edifice boundaries using DEMs and applying minimum cost flow networks. The algorithm, based on the premise that volcano edifices are bounded by concave breaks in slope, calculates the best possible outline by solving a minimum cost flow problem. Thus, it delimits only the edifice as a specific landform and excludes the surrounding apron and other far reaching products. Application of the algorithm is intended for any volcano with recognizable positive topography, independently of its size. The paper is organized as follows. Section 2 describes the proposed algorithm. Evaluation of the algorithm by real data is presented in Section 3. Conclusions are presented in Section 4.

2. The NETVOLC algorithm

2.1. Rationale

The general problem is to compute a closed path around a volcanic center that represents the edifice boundary. Considering a DEM of an idealized volcanic cone emerging over an arbitrary landscape, we can define a closed path by intersection of the cone surface with the pre-cone landscape surface. This outline represents the edifice boundary (Fig. 1) and is precisely located by concave breaks in slope: points with maximum negative profile curvature. Thus, the straightforward solution for a DEM of the area is to identify pixels representing concave breaks in slope around the edifice base.

There are several ways to measure the breaks in slope of a surface. The profile curvature of a surface can be computed by intersecting it with the plane of the z axis and aspect direction (Evans, 1980; Wood, 1996). The resulting measure is known as *profile convexity*, the rate of slope change along the vertical axis. Values of *profile convexity* range from negative on concave surfaces to positive on convex surfaces. In an ideal case, a volcanic edifice boundary is well represented by pixels with maximum concavity (most negative profile convexity), thus rendering additional information unnecessary.

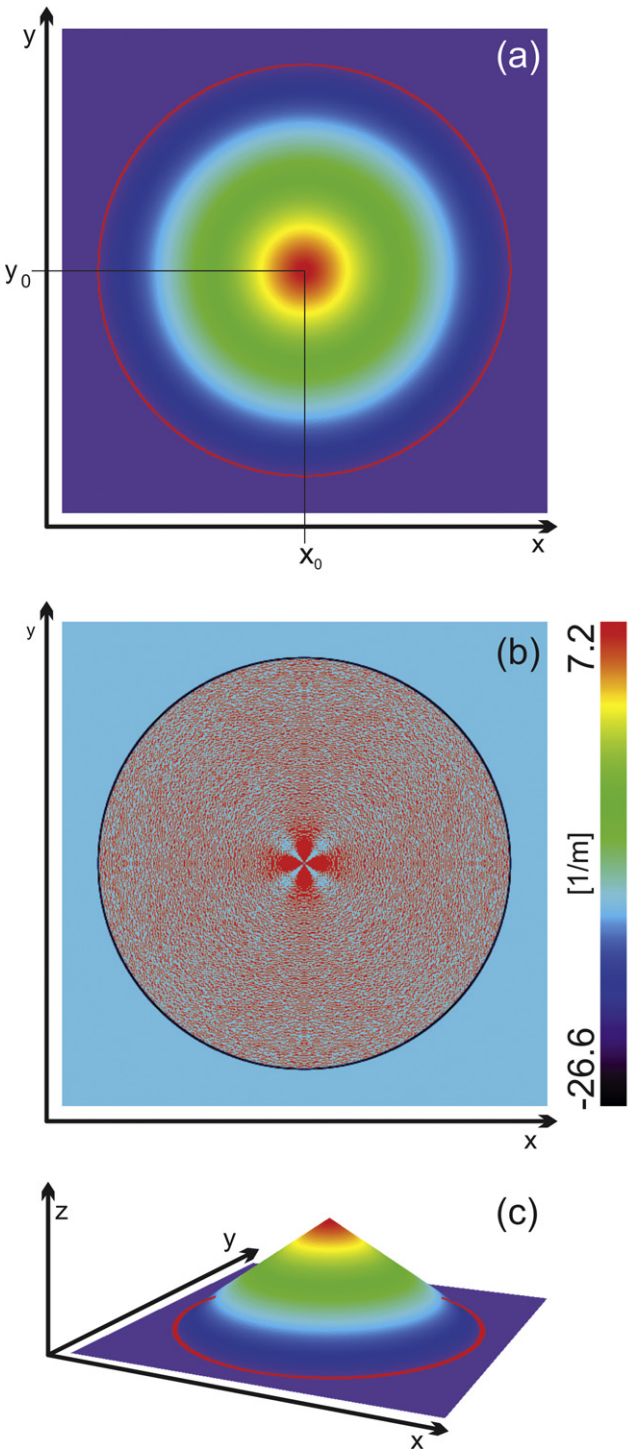

Fig. 1. DEM of an idealized volcanic cone. (a) is the xy plane of the DEM; point ($x0$, $y0$) is the center of the edifice. (b) is the profile convexity map of the DEM in 1/m units. (c) is a 3D-plot of the DEM. The red outline in (a) and (c) represents the volcanic edifice boundary; it is perfectly defined by concave breaks in slope represented by the most negative values in (b). Cross pattern around the cone apex in (b) is a processing artifact never observed in real cases. (For interpretation of the references to color in this figure legend, the reader is referred to the web version of this article.)

In reality, volcanic edifices are more complex. They are shaped by several natural processes, both internal and external (erosion, collapse, activity from nearby volcanoes, etc.), that complicate their form and obscure the boundaries. Thus, boundary delimitation may require additional information such as aspect, slope and elevation. Aspect particularly, is a significant DEM-derivative product as it can

discriminate between concave breaks in slope facing outward or inward from the volcanic center. Inward-facing surfaces may indicate the presence of craters, erosional features, or the base of neighboring edifices. Slope angle can be used to discriminate breaks in surface slope at high gradients near the edifice summit from the lower gradient breaks in slope at the base. Elevation can filter out undesirable complexities in the summit region and/or below the base.

The edifice boundary problem can be conceptualized as a flow minimization problem in a network that can be efficiently solved by employing minimum cost flow (MCF) algorithms (Ahuja et al., 1993). We propose optimizing an objective function obtained from a DEM and its derived morphometric layers, directly profiting from the relation between edifice boundary and maximum concavity. Thus, NETVOLC is essentially a computer tool for defining edifice boundaries, based in a MCF algorithm and DEM derived data.

2.2. Procedure

Fig. 2 shows a schematic flow chart of the implemented procedure. The necessary inputs are: (a) a DEM covering the volcano; and (b) the *xy* location of a point approximating the center of the volcano. From the DEM, three layers are derived using the method proposed by Wood (1996) and implemented in the ENVI software: profile convexity, slope, and aspect. Next, we compute an ideal cone with apex located at the central point and calculate an aspect layer from it. Subtracting this model aspect layer from the real (measured) aspect values, we obtain a differential aspect layer that indicates the direction in which pixels are facing: outward from the central point (pixels with an aspect difference <90 degree) or inward (pixels with an aspect difference >90 degree).

Then, the profile convexity and differential aspect layers are combined into a binary mask called *azimuthal curvature*:

$$Azimuthal\ curvature = \begin{cases} 1, & Profile\ convexity < 0 \quad \text{and} \quad \text{aspect } D_{\text{if}} < 90^{\circ} \\ 0, & \text{otherwise} \end{cases} \tag{1}$$

Pixels with values of 1 (those with a concave profile convexity and facing outward from the volcanic center) are considered "good", whereas pixels with values of 0 are discarded. *Azimuthal curvature* thus limits the set of possible pixels composing the desired solution and the problem is reduced to computing the best possible closed path around the central point linking a set of these pixels.

The automatic path computation is implemented by a MCF network algorithm. The network is composed of N nodes (or vertices) and E undirected edges linking the nodes. We generate the network by Delaunay triangulation considering all pixels of the *azimuthal curvature* mask having values of 1 as nodes. Every edge $e_{i,j}$ linking the nodes is associated with a function value; it represents the charge (or cost) of using that edge for going to a node j from a node i, and is expressed as the cost $c_{i,j}$ of the edge $e_{i,j}$. Nodes n are associated with a quantity b that represents a deficit or a surplus that must be balanced. A node n is usually called a *supply node* when b is positive, a *demand node* when b is negative, or a *transient node* when b is zero.

If the network presents a node imbalance (wherein supply and/or demand nodes exist), the aim of MCF algorithms is to balance the network computing an optimal solution so that:

$$\min \sum_{e_{i,j}} c_{i,j} f_{i,j} \tag{2}$$

where $c_{i,j}$ is the cost of making use of the edge $e_{i,j}$, and $f_{i,j}$ is the times that the edge $e_{i,j}$ has been used (in our case never more than once). The problem formulation (2) is subject to the following restrictions:

$$\sum_{e_{i,j}} f_{i,j} - \sum_{e_{j,i}} f_{j,i} = b_i \quad \forall i \in N \tag{3a}$$

$$f_{i,j} \le u_{i,j} \quad \forall e_{i,j} \in E \tag{3b}$$

where $u_{i,j}$ represents the transport capacity of the edge $e_{i,j}$. Note that transport capacity is an edges' property that depends on the nature of the problem. In our case it is initially set to 1 for all edges.

We use an implementation of the primal/dual network simplex algorithm (Loebel, 2004) to solve the optimization problem. An in-depth explanation of MCF algorithms is outside of the scope of this work, but a complete description can be found in Ahuja et al. (1993).

The cost function (and resulting *cost map*) is defined for every pixel using the DEM-derived morphometric layers. We propose one main cost function and three alternative more complex functions for greater algorithm flexibility:

$$Cost\ map = -\frac{1}{(Profile\ \ convexity)}, \quad \{Azimuthal\ \ curvature = 1 \tag{4a}$$

$$Cost\ \ map = -\frac{1}{(Profile\ \ convexity)}, \times \begin{cases} Azimuthal\ \ curvature = 1 \quad \text{and} \\ \begin{pmatrix} Spatial\ \ extent > Min\ \ threshold \\ Spatial\ \ extent < Max\ \ threshold \end{pmatrix} \quad \text{or/and} \end{cases} \tag{4b}$$

$$Cost\ map = -\frac{1}{(Profile\ \ convexity)} + Slope, \quad \{Azimuthal\ curvature = 1 \tag{4c}$$

$$Cost\ map = -\frac{1}{(Profile\ \ convexity)} + Slope, \times \begin{cases} Azimuthal\ curvature = 1 \quad \text{and} \\ \begin{pmatrix} Spatial\ extent > Min\ threshold \\ Spatial\ extent < Max\ threshold \end{pmatrix} \quad \text{or/and} \end{cases} \tag{4d}$$

where *spatial extent* is a factor that considers elevation above sea level and/or radial distance from the approximate center of the volcano, *Slope* is the slope gradient measured in degrees (with the convention of 0 degrees for an horizontal plane), and *Min threshold* and *Max threshold* are user-defined spatial extent limits. Profile convexity and aspect are the most relevant parameters and are considered in all of the functions. Which cost function is applied will depend on the complexity of the volcanic terrain. For most cases the main cost function (4a), which depends only on profile convexity and aspect, can be used satisfactorily. Where there are breaks in slope at high gradients within the edifice, function (4c) is preferred so that these unwanted inner breaks in slope are minimized with respect to the desired outer breaks in slope. Functions (4b) and (4d) include elevation and/or radial distance thresholds to exclude undesirable complex areas that can disturb the solution (see Section 3 for application of the cost functions).

The desired solution must fulfill two conditions: (1) it must start and end at nodes that share an edge; (2) it must form a closed path around the central point. Finding a solution that fulfills both conditions in a Cartesian system implies that we would have to impose some difficult-to-implement restrictions such as forcing intermediate pixels to be reached around the volcanic center, imposing a minimal path length, etc. We avoid this issue by solving the minimization problem in polar coordinates. To do so, we transform the *azimuthal curvature* grid to a polar coordinate

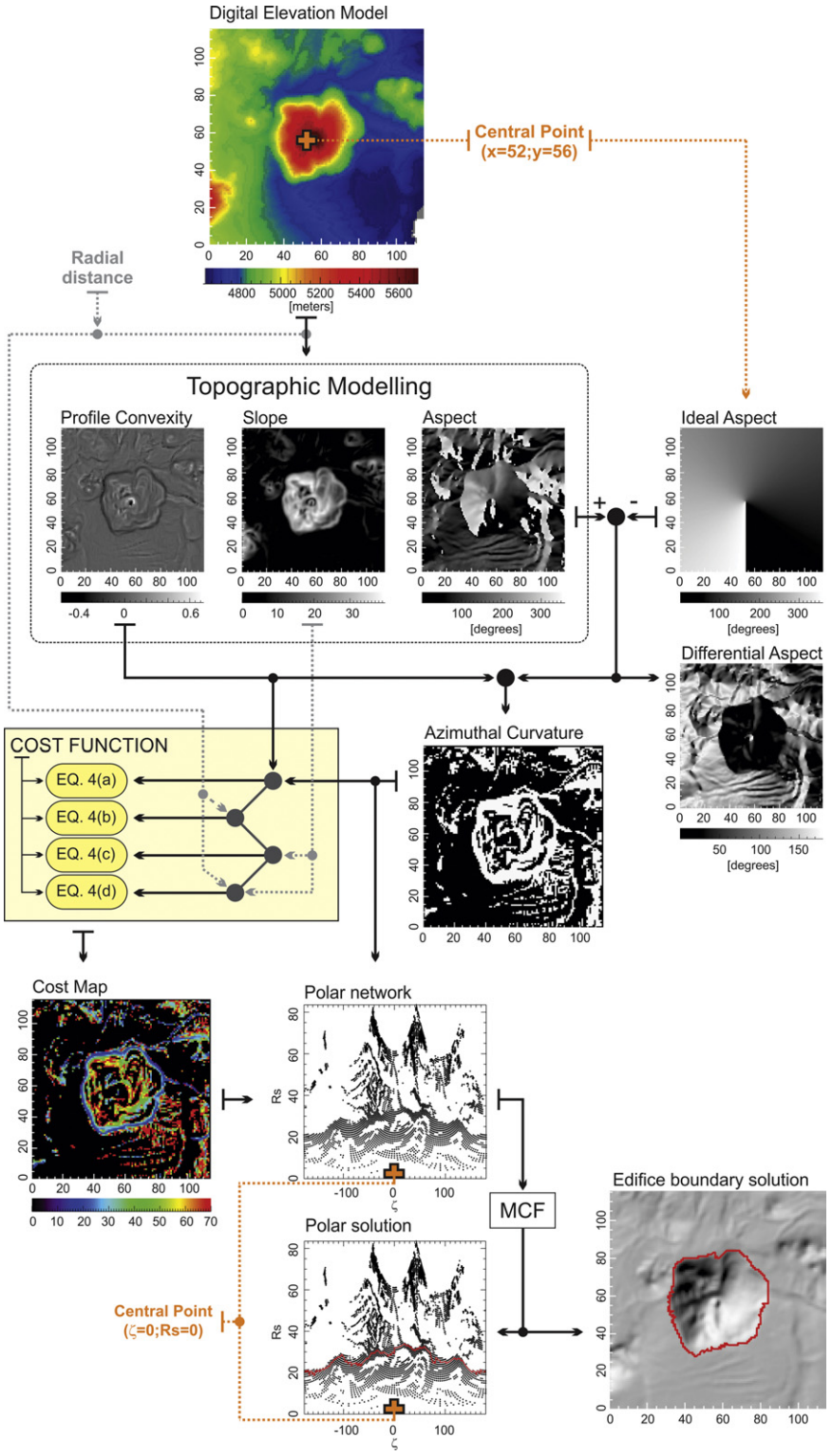

Fig. 2. Schematic flow chart of the implemented procedure for computation of volcanic edifice boundaries. Chascón volcano (Central Andes, Chile) is the example; DEM is the 90 m SRTM DEM.

system centered at the central point. Thus, the starting pixel has coordinates $R_s = r$ and $\vartheta_s = -180$ degrees, and the ending pixel has coordinates $R_e = r$ and $\vartheta_e = 180$ degrees. The main advantage of this approach is that the path computed between the start and the end pixel will necessarily wrap around the central point, located at ($\vartheta_c = 0$; $R_c = 0$).

Once the polar network is assembled, the cost associated to every edge $e_{i,j}$ is defined as:

$$c_{i,j} = \left(\frac{CostMap\_i + CostMap\_j}{2}\right) \times le_{i,j}^2 \tag{5}$$

where *CostMap_i* and *CostMap_j* are the pixels' cost extracted from a selected function (4a)–(4d), and $le_{i,j}$ is the Euclidean length of the edge $e_{i,j}$ between nodes i and j.

The network imbalance is imposed manually. To avoid user subjectivity in the selection of the imbalanced nodes we create two fictitious nodes: a *supply node* connected to every node on the −180 degrees azimuth polar coordinate; and a *demand node* connected to every node on the 180 degrees azimuth polar coordinate. This strategy has the following advantages: (1) the selection of nodes depends exclusively on the cost function; (2) the computed path between the fictitious nodes is always around the volcanic center.

As an initial step, we analyze the network for overcoming undesired situations presented when the edges linking the supply and demand nodes are few. Under this condition, the network solver will give priority to these edges (independently of their associated cost) and the solution will be undoubtedly wrong. In particular, there are two kinds of edges that can produce this scenario: (1) the edges linking the four corners of the network grid, and (2) those edges belonging to the triangulation convex hull (Knuth, 1992). The latter is easily identified and cancelled from the network when the triangulation is computed. Identifying the former is more difficult but can be done because it is characterized by edges that are much longer than the typical ones found within a given network. A simple statistical analysis based on the length of edges is implemented to identify and remove them.

The suggested algorithm gives accurate solutions for most simple cases. Inconveniently, however, it tends to compute the shortest path between the fictitious nodes. In boundary delimitation problems a shortest path is not always the best solution. We find that a better solution than (2) is:

$$\min \frac{\sum_{e_{i,j}} c_{i,j} f_{i,j}}{n} \tag{6}$$

where n is the number of nodes used in the global solution. The new problem formulation (6) is thus a normalized solution.

Computing (6) is not simple because the number of nodes in the final solution is a-priori unknown. To overcome this limitation we propose an iterative mechanism that searches for several solutions. Every solution is a combination of several edges; and every edge is associated with a cost given by Eq. (5). A way to alter the computed MCF solution without changing the cost of the edges is to modify their transport capacity $u_{i,j}$. The proposed iterative mechanism is based on the statistics of the edges' costs in the previous computed solution. Those edges with costs above a threshold computed from the mean and the standard deviation of the previous solution are cancelled from the network by assigning a null transport capacity $u_{i,j}=0$. In the following iteration, a new solution is computed considering the modified network. Note that in this way we favor the shorter edges (see Eq. (5)) over the longer ones, whose costs tend to be higher due to the parameter $le_{i,j}$. The steps of the iteration procedure can be summarized as:

a) An initial solution is computed using formulation (2).
b) The mean ($\bar{x}$) and the standard deviation (σ) of the edges' costs included in the solution are computed.
c) Assuming that the best edges are those with costs below the range $x<\bar{x}+2\sigma$, edges above this range are cancelled from the network.
d) A new optimal solution is computed considering the remaining edges.
e) The whole procedure is repeated until a finite number of solutions are reached (from testing we find that 10 iterations are enough to reach a satisfactory solution).
f) Considering formulation (6), the total cost of each solution is normalized by the corresponding number of nodes.
g) The solution with the lowest normalized cost is the solution of the problem.

The procedure is illustrated in Figs. 3–5. Fig. 3 shows the *cost map* in Cartesian coordinates (a) and the network in polar coordinates (b). Fig. 4 is a detail of the network (red box in Fig. 3) showing a portion of the solutions reached in three successive iterations (yellow lines) and the cancelled edges of the previous iterations (red segments). Fig. 5 shows the solutions obtained after iterations 1 to 3 and the final solution (in red).

A final control over the computed solution must be applied. As shown in Fig. 5, the starting and ending pixels of the solutions can be disconnected; this occurs when the MCF algorithm computes a solution where the starting and ending pixels are not equidistant from the origin ($R_s=0$). In order to obtain a continuous solution, we adjust it by two additional computations. First, we constrain the ending node to the same coordinate as the starting node. Second, we constrain the starting node to the same coordinate as the ending one. Both additional solutions are compared and the one with lower normalized cost is selected.

3. Algorithm evaluation

In this section we apply NETVOLC to the Mauna Kea pyroclastic cone field (Hawaii, USA) in order to evaluate performance of the

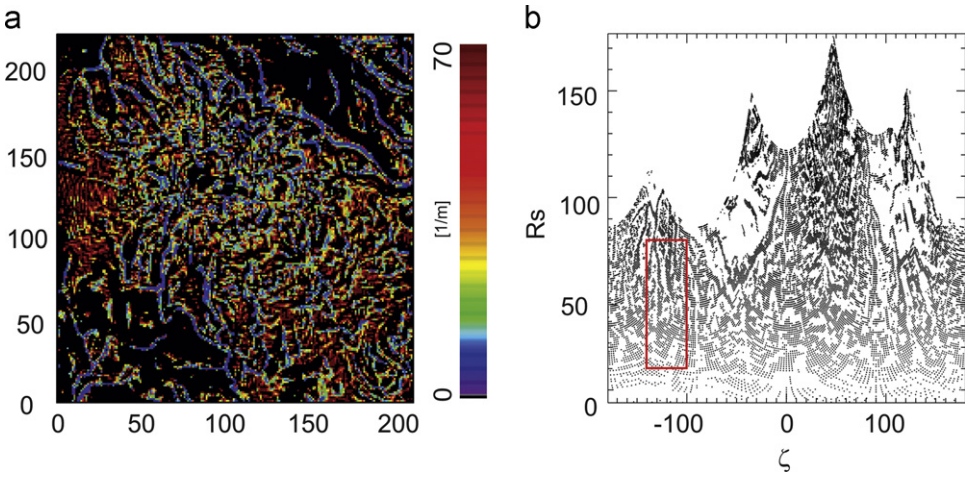

Fig. 3. Inputs for the iterative procedure of volcanic edifice boundary computation. (a) is the cost map obtained from the DEM-derived morphometric layers. (b) is the polar distribution of the network pixels. Chimborazo volcano (Ecuador) is the example; DEM is the 90 m SRTM DEM.

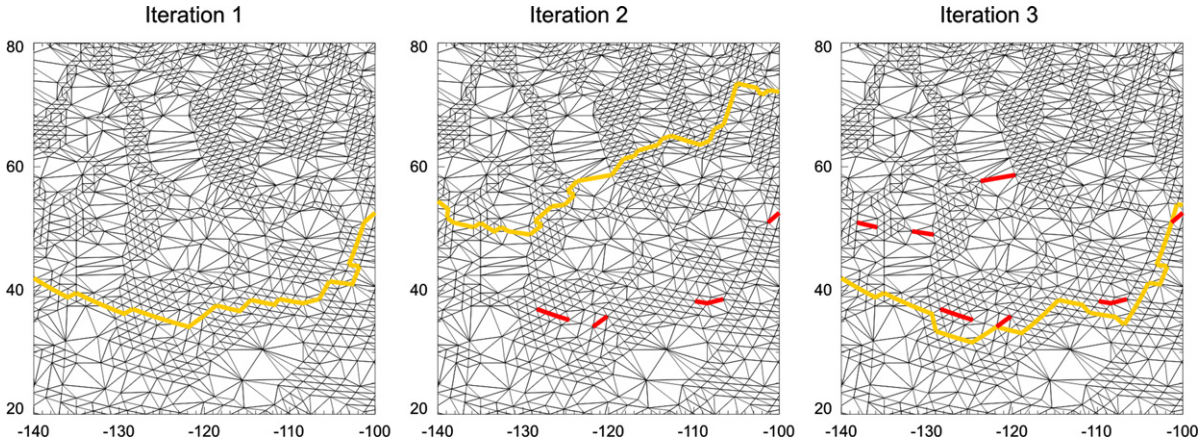

Fig. 4. Illustration of the iterative procedure for computation of volcanic edifice boundaries. The network is a computed Delaunay triangulation corresponding to the area enclosed by the red box in Fig. 3(b). Iteration 1, 2 and 3 are the first three iterations of the procedure. The yellow line represents part of the computed solution. On iterations 2 and 3, the cancelled edges of the previous iterations are shown in red. (For interpretation of the references to color in this figure legend, the reader is referred to the web version of this article.)

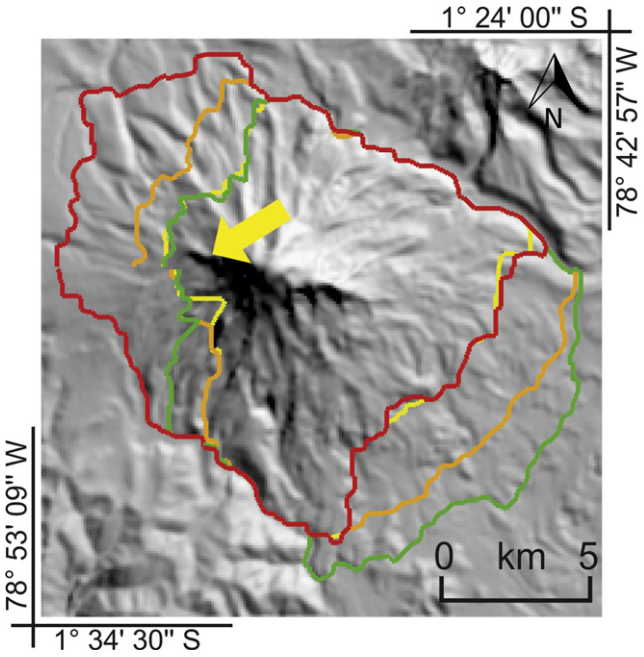

Fig. 5. Computed solutions for Chimborazo volcano. Yellow, orange and green outlines are the solutions corresponding to the first, second and third iterations, respectively. Red outline is the best solution reached at iteration 4. The yellow arrow indicates location of discontinuities between the starting and ending pixels for the first three iterations; this problem is resolved for the final solution (see text). (For interpretation of the references to color in this figure legend, the reader is referred to the web version of this article.)

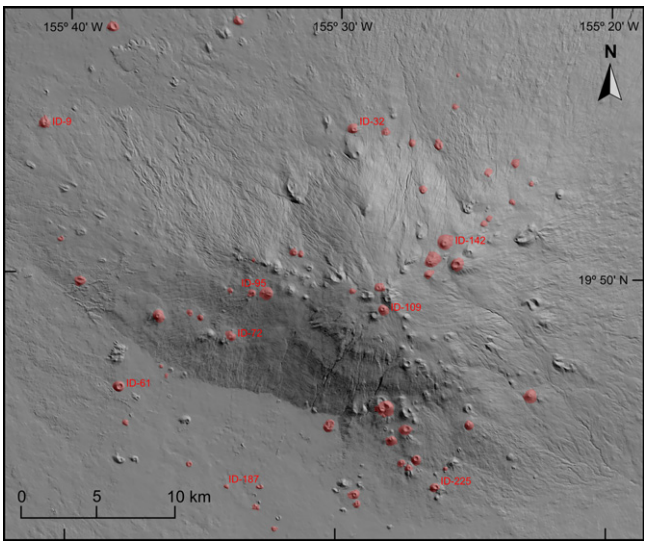

Fig. 6. NED DEM-derived shaded-relief image of the Mauna Kea cone field (Hawaii, USA) highlighting the 56 cones analyzed with the NETVOLC algorithm. Cones with ID's are those shown in Fig. 9.

algorithm. The Mauna Kea cone field contains hundreds of cones with a wide range of morphologies and is covered by the 10 m National Elevation Dataset (NED) DEM (Gesch et al., 2002; Maune, 2007). Furthermore, Kervyn et al. (2012) recently carried out a morphometric analysis of this cone field using the NED DEM and considering slope breaks as the key criteria for manual delineation of the cone outlines. We here compare the NETVOLC results with the manual outlines of Kervyn et al. (2012).

We applied the algorithm to 56 cones (Fig. 6), all of which are included by Kervyn et al. (2012) in a subset of cones with 'representative morphologies'. For comparison with manual outlines, two widely used morphometric parameters are evaluated, average cone base width (W_{CO}) and cone height (H_{CO}), together with their ratio, H_{CO}/W_{CO} (e.g. Wood, 1980). W_{CO} is directly derived from the area enclosed by the base outline since it is calculated as the diameter of an area-equivalent circle. H_{CO} is estimated as the difference between the maximum cone elevation (the same value for both manual and NETVOLC analysis since the same DEM was used) and the average elevation of the base outline. The morphometric parameters obtained from NETVOLC and manual outlines are shown in Tables 1–4 (supplementary material) and plotted in Figs. 7 and 8. Fig. 9 shows examples of the outlines.

Visual inspection of outlines obtained using the main cost function (Eq. (4a)) suggests three different groups of NETVOLC outlines as compared with the manual ones that depend on cone morphology and on the topography of its surroundings:

– Group I (21 cones; Table 1): the NETVOLC outlines follow the same slope break paths around the cones as the manual outlines. Outlines are thus quite similar, although the NETVOLC outlines tend to cover a smaller area because they are 'tighter' around the cone (Fig. 9a). Consequently, the derived NETVOLC parameters have somewhat smaller values than the manual parameters (Figs. 7 and 8), with W_{CO} and H_{CO} differences mostly between 0% and −10% (5% average absolute difference

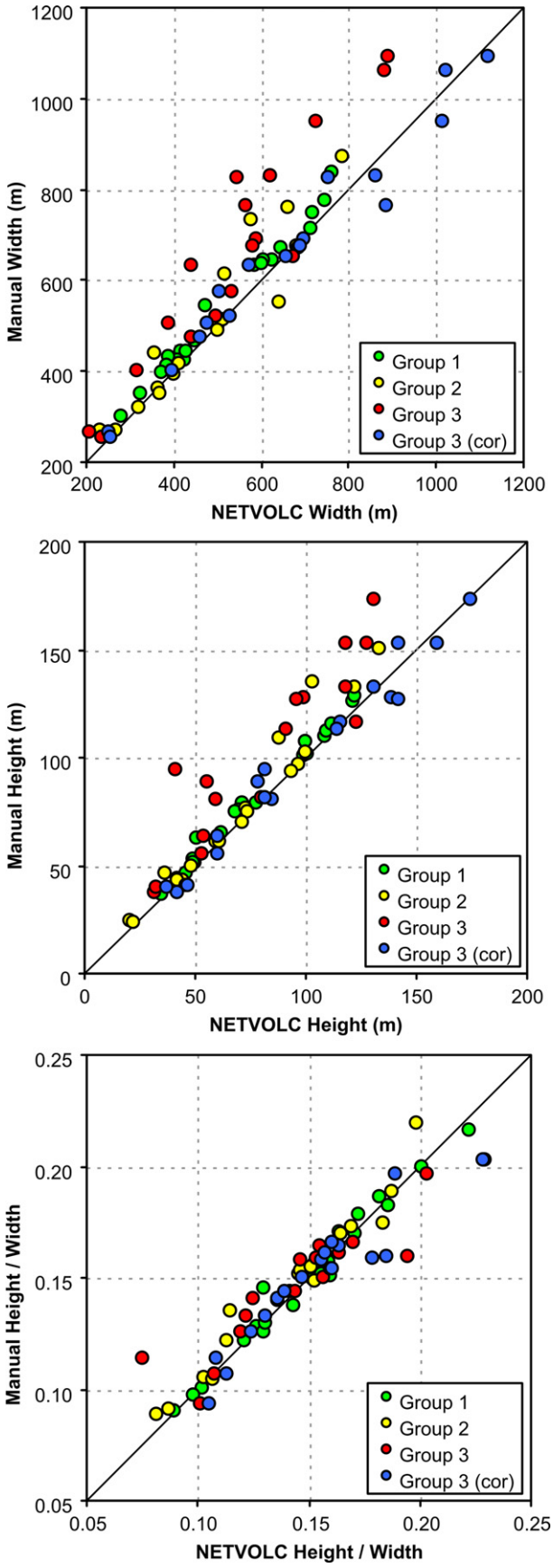

Fig. 7. XY plots comparing morphometric parameters obtained from the NETVOLC with the manual (Kervyn et al., 2012) outlines for 56 cinder cones of the Mauna Kea cone field (Hawaii, USA).

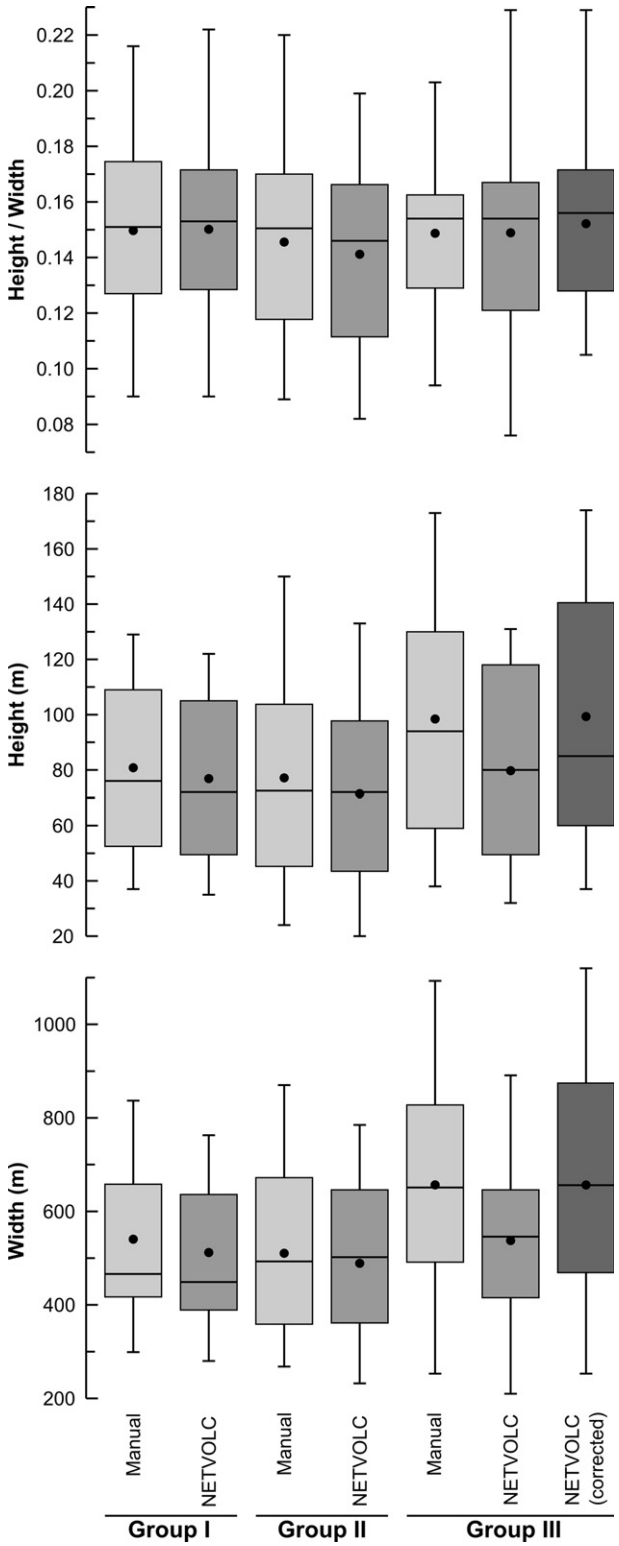

Fig. 8. Box-and-whisker plots summarizing the statistics of the morphometric parameters obtained from the NETVOLC and manual (Kervyn et al., 2012) outlines for the analyzed cones of the Mauna Kea cone field (Hawaii, USA). Bottom and top of box are the lower and upper quartiles, respectively; inner horizontal line is the median; inner dot is the mean; whiskers are minimum and maximum values.

for both parameters). The differences in width and height between outlines correlate directly, and thus the H_{CO}/W_{CO} ratios are very similar, with differences mostly below 6% (2.5% average absolute difference). From our testing of the

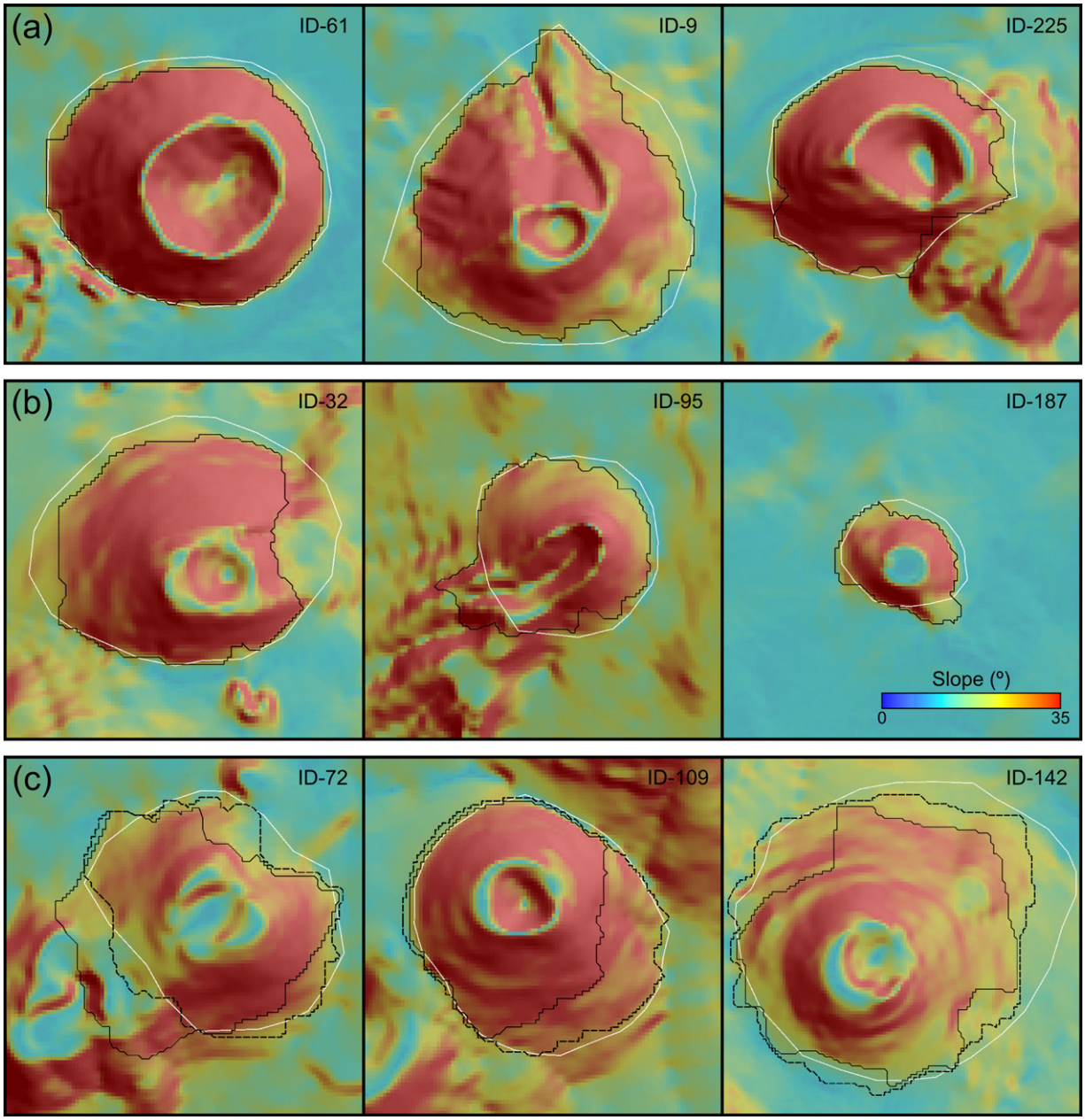

Fig. 9. Examples of the computed NETVOLC outlines using the main cost function (black) and comparison with the manual outlines (white) traced by Kervyn et al. (2012); (a) are Group I cones; (b) are Group II cones; (c) are Group III cones, where dashed black outlines are the corrected NETVOLC outlines using alternative cost functions. Images are slope layer draped over shaded-relief layer. Extent of each box is 1 km.

NETVOLC algorithm on stratovolcanoes, we also find that resulting outlines are generally 'tighter' than manual outlines. Cones of this group have mostly steep flanks with well defined slope-breaks at their bases and are located on relatively uniform topography. These NETVOLC outlines, using the main cost function, are accurate and it can be argued that they are better than the manual outlines as they follow more precisely the slope breaks.

– Group II (18 cones; Table 2): the NETVOLC outlines follow mostly the same slope break paths as the manual outlines, but parts of the outlines do not coincide (Fig. 9b). The NETVOLC outlines show differences in W_{CO} between −21% and +16%, and in H_{CO} between −24% and +2% (7% average absolute difference for both parameters) compared to the manual outlines (Figs. 7 and 8). Differences in the H_{CO}/W_{CO} ratios are mostly below 10% (4% average absolute difference). Cones of this group are mostly well defined but contain complexities that produce different possible slope-break paths; surroundings are relatively uniform. In these cases, both outlines may be valid; the NETVOLC outlines are more accurate in terms of following the strongest possible slope breaks, but interpretation may be needed to decide which path is best.

– Group III (17 cones; Table 3): the NETVOLC outlines follow slope-break paths that are partially or totally not around the cone base. The outlines and derived parameters show the greatest differences with the manual outlines (Figs. 7, 8 and 9c). Differences in W_{CO} are between −34% and +3% (17% average absolute difference), and in H_{CO} between −56% and +14% (19% average absolute difference); differences in H_{CO}/W_{CO} ratios are between −33% and +22% (8% average absolute difference). Inaccuracies in the NETVOLC outlines are due to different causes. In most cones of this group the NETVOLC outlines

are too high up on the cone, following slope breaks at steep gradients (Fig. 9c). We have found during testing of the algorithm on stratovolcanoes, using other DEMs, that slope breaks at high gradients well within the edifice are quite common, and can be a problem for NETVOLC. In the present case, such slope-breaks are mostly artifacts of the NED DEM that are generated during interpolation of elevation contours. On other cones, inaccuracy arises when the algorithm follows slope breaks on a neighboring landform and not to the subject cone, such as a coalescing cone (Fig. 9c) or a valley. For all these problematic cases, we re-applied the algorithm using the alternative cost functions (Eq. (4b)–(4d)) and obtained a set of corrected outlines (Table 4). These new outlines agree much better with the manual outlines (Figs. 7, 8 and 9c), showing differences in W_{CO} between −12% and +16% (5% average absolute difference), and in H_{CO} between −13% and +17% (7% average absolute difference); differences in H_{CO}/W_{CO} ratios are between −5% and +16% (5% average absolute difference).

Considering the outlines obtained using the main cost function for the cones of groups I and II, and the corrected outlines using the alternative cost functions for the cones of group III, the average absolute differences in the derived parameters compared with the manual outlines are 6% for W_{CO} and H_{CO}, and 4% for H_{CO}/W_{CO}. The average values are W_{CO}=566 m; H_{CO}=85 m; H_{CO}/W_{CO} 0.1480 for the manual outlines, and W_{CO}=548 m; H_{CO}=82 m; H_{CO}/W_{CO}= 0.1477 for the NETVOLC outlines.

In summary, approximately 2/3rds of the analyzed cones delivered a good outline from the main cost function of NETVOLC. At the remaining 1/3rd of cones, the outlines obtained from the main cost function are partially or totally inaccurate. Causes include slope breaks within cones at high gradients or disturbance of slope breaks from neighboring landforms. For these cases, good outlines can be obtained by applying an alternative cost function. A further source of error is the artificial steps or terraces in the NED DEM, a common problem in topo-derived DEMs. Correction of the DEM to eliminate or attenuate these artifacts should be performed prior to applying NETVOLC. The NETVOLC outlines compare well with manual outlines. The outlines follow mostly the same slope-break paths around the cone bases; partially different outlines can occur when the cone bases have complexities that produce more than one possible slope-break path. Compared to manual outlines, the NETVOLC outlines are generally tighter around the cones. Thus, the derived morphometric parameters W_{CO} and H_{CO} tend to have smaller values, but differences are generally below 10%. Because width and height correlate, the H_{CO}/W_{CO} ratio varies less, and differences are generally below 6%. It can be argued that the obtained NETVOLC outlines are in most cases better than manual outlines because they follow more accurately the slope breaks around the cone bases.

4. Conclusions

NETVOLC is an innovative algorithm for automatically computing the boundary of volcanic edifices. It has the advantage of being more objective and much faster than manual delineation, and requires only a DEM of the volcano as input. In most cases, the main cost function produces accurate outlines, but can yield erroneous results for complex edifices. The alternative cost functions give the flexibility to re-process these cases and obtain good results, although this implies that results have to be inspected and the alternative function has to be selected by the user, introducing some subjectivity and semi-automation. Future development towards eliminating this drawback is needed. Still, NETVOLC is, at present, more objective and less time-consuming than the manual alternative.

As formulated, the proposed algorithm is straightforward to apply on individual volcanoes. Boundary delimitation on cone fields (as presented above) constitutes a repetitive task where each volcano must be identified and processed. In these cases, a combination of an alternative approach, such as the closed-contouring method, together with NETVOLC could be applied, where closed-contour solutions would be used as input for NETVOLC. In such a case, NETVOLC would act as a corrective method of closed-contouring solutions, being a valid alternative to that proposed by Bohnenstiehl et al. (2012). This approach would allow rapid processing of large areas with numerous volcanoes and minimal human intervention.

Although intended for volcano edifices, NETVOLC can also be used on other landforms with similar concave break-in-slope boundaries such as drumlins or hummocks of varied origins. Furthermore, straightforward modifications can be implemented to extend the algorithm's capabilities for delimiting landforms bounded by convex breaks-in-slope, such as summit craters and calderas.

Finally, for a given volcano or cone field, DEMs with higher resolution and accuracy will become available as new sensors and technologies emerge. NETVOLC provides a flexible tool for profiting from such new DEMs without much effort in re-drawing the volcano outlines.

Acknowledgments

Matthieu Kervyn is thanked for kindly providing his manual outlines and resulting data of the Mauna Kea cone field. Reviewers Richard J. Pike and Ian S. Evans are acknowledged for their very insightful comments and corrections to the original manuscript. Pablo Grosse acknowledges CONICET and Fundación Miguel Lillo for their support.

Appendix A. Supplementary information

Supplementary data associated with this article can be found in the online version at http://dx.doi.org/10.1016/j.cageo.2013.03.011.

References

Ahuja, R.K., Magnanti, T.L., Orlin, J.B., 1993. Network Flows: Theory, Algorithms, and Applications, first ed. Prentice Hall.
Behn, M.D., Sinton, J.M., Detrick, R.S., 2004. Effect of the Galápagos hotspot on seafloor volcanism along the Galápagos spreading center (90.9–97.6°W). Earth and Planetary Science Letters 217, 331–347.
Bohnenstiehl, D.R., Howell, J.K., Hey, R.N., 2008. Distribution of axial lava domes along a superfast overlapping spreading center, 27–32°S on the East Pacific Rise. Geochemistry, Geophysics, Geosystems 9, Q12016.
Bohnenstiehl, D.R., Howell, J.K., White, S.M., Hey, R.N., 2012. A modified basal outlining algorithm for identifying topographic highs from gridded elevation data, Part 1: Motivation and methods. Computers & Geosciences 49, 308–314.
Bue, B.D., Stepinski, T.F., 2006. Automated classification of landforms on Mars. Computers & Geosciences 32, 604–614.
Drăguţ, L., Blaschke, T., 2006. Automated classification of landform elements using object-based image analysis. Geomorphology 81, 330–344.
Evans, I.S., 1972. General geomorphometry, derivatives of altitude, and descriptive statistics, in: Spatial Analysis in Geomorphology. Harper & Row, Great Britain17–90.
Evans, I.S., 1980. An integrated system of terrain analysis and slope mapping. Zeitschrift fur Geomorphologie 36 (Suppl. Bd), 274–295.
Evans, I.S., 2012. Geomorphometry and landform mapping: what is a landform? Geomorphology 137, 94–106.
Favalli, M., Karátson, D., Mazzarini, F., Pareschi, M.T., Boschi, E., 2009. Morphometry of scoria cones located on a volcano flank: a case study from Mt. Etna (Italy),

based on high-resolution LiDAR data. Journal of Volcanology and Geothermal Research 186, 320–330.
Gesch, D., Oimoen, M., Greenlee, S., Nelson, C., Steuck, M., Tyler, D., 2002. The National Elevation Dataset. Photogrammetric Engineering and Remote Sensing 68, 5–11.
Grosse, P., van Wyk de Vries, B., Euillades, P.A., Kervyn, M., Petrinovic, I.A., 2012. Systematic morphometric characterization of volcanic edifices using digital elevation models. Geomorphology 136, 114–131.
Grosse, P., Vries, B., van, W. de, Petrinovic, I.A., Euillades, P.A., Alvarado, G.E., 2009. Morphometry and evolution of arc volcanoes. Geology 37, 651–654.
Hillier, J.K., 2008. Seamount detection and isolation with a modified wavelet transform. Basin Research 20, 555–573.
Howell, J.K., White, S.M., Bohnenstiehl, D.R., 2012. A modified basal outlining algorithm for identifying topographic highs in gridded elevation data, part 2: Application to Springerville Volcanic Field. Computers & Geosciences 49, 315–322.
Iwahashi, J., Pike, R.J., 2007. Automated classifications of topography from DEMs by an unsupervised nested-means algorithm and a three-part geometric signature. Geomorphology 86, 409–440.
Karátson, D., Telbisz, T., Wörner, G., 2012. Erosion rates and erosion patterns of neogene to quaternary stratovolcanoes in the Western Cordillera of the Central Andes: an SRTM DEM based analysis. Geomorphology 139-140, 122–135.
Kervyn, M., Ernst, G.G.J., Carracedo, J.-C., Jacobs, P., 2012. Geomorphometric variability of "monogenetic" volcanic cones: evidence from Mauna Kea, Lanzarote and experimental cones. Geomorphology 136, 59–75.
Knuth, D.E., 1992. Axioms and Hulls. Springer-Verlag, Berlin; New York.
Loebel, A., 2004. MCF Version 1.3—A network simplex implementation. Available for Academic Use Free of Charge at ⟨www.zib.de⟩, Berlin, Germany.
Maune Ph D, D.F. (Ed.), 2 Har/Dvdr. ed. Asprs Pubns.
Neuendorf, K.K.E., Mehl, J.P.J., Jackson, J.A. (Eds.), 2005. fifth ed. American Geological Institute.
Pike, R.J., 1978. Volcanoes on the inner planets—some preliminary comparisons of gross topography. In: Lunar and Planetary Science Conference Ninth, Houston, Texas, March 13–17: Proceedings, Vol. 3, Pergamon Press, New York, pp. 3239–3273.
Plescia, J.B., 2004. Morphometric properties of Martian volcanoes. Journal of Geophysical Research 109, E03003.
Saha, K., Wells, N.A., Munro-Stasiuk, M., 2011. An object-oriented approach to automated landform mapping: a case study of drumlins. Computers & Geosciences 37, 1324–1336.
Schneider, M., Klein, R., 2010. Semi-automatic digital landform mapping. In: Otto, J.-C., Dikau, R. (Eds.), Landform—Structure, Evolution, Process Control, Lecture Notes in Earth Sciences. Springer Berlin, Heidelberg, pp. 37–51.
Smith, M.J., Clark, C.D., 2005. Methods for the visualization of digital elevation models for landform mapping. Earth Surface Processes and Landforms 30, 885–900.
Völker, D., Kutterolf, S., Wehrmann, H., 2011. Comparative mass balance of volcanic edifices at the southern volcanic zone of the Andes between 33°S and 46°S. Journal of Volcanology and Geothermal Research 205, 114–129.
Wood, C.A., 1980. Morphometric evolution of cinder cones. Journal of Volcanology and Geothermal Research 7, 387–413.
Wood, J.D., 1996. The Geomorphological Characterization of Digital Elevation Models. Ph.D. Thesis. (University of Leicester, UK, ⟨http://www.soi.city.ac.uk/~jwo/phd⟩).